JOURNAL OF MATERIALS SCIENCE **38** (2003) 1377–1381

Laser-induced self-propagating reaction synthesis of amorphous-based composite Zr-Al-Ni-Cu alloys

CUNSHAN WANG, LINHUI GAO, GANG LI, YANFANG WANG, YUANLIANG XIA
Key State Laboratory for Materials Modification by Laser, Ion, and Electron Beams, Dalian University of Technology, Dalian 116023, People's Republic of China
E-mail: laser@dlut.edu.cn

S. BYSAKH
Department of Metallurgy, Indian Institute of Science, Bangalore 100560, India

CHUANG DONG
Key State Laboratory for Materials Modification by Laser, Ion, and Electron Beams, Dalian University of Technology, Dalian 116023, People's Republic of China

Strong exothermic reaction due to large negative enthalpy of mixing can occur among major components of bulk metallic glass forming alloy systems. Based on this idea, we developed a new technique to fabricate amorphous-based composite materials using Laser-induced Self-propagating Reaction Synthesis (LSRS). The LSRS of the $Zr_{55}Al_{10}Ni_5Cu_{30}$ alloy shows that the products mainly consist of the amorphous, Zr_3Al_2 and Zr_2Cu phases. Hardness and wear resistance of the produced composite alloys are measured and are compared to the single amorphous phase alloy of the same composition.

1. Introduction

In recent years, there have constantly been breakthroughs in the research of bulk amorphous alloys. The amorphous alloys with large glass-forming ability have been found in a number of alloy systems such as Zr-Al-TM, Ln-Al-TM, Ti-Zr-TM, Mg-Ln-TM and Fe-(Al, Ga)-(P, B, C, Si) [1, 2]. These amorphous alloys have been produced by various solidification methods such as copper mold casting, high-pressures die casting, water quenching and unidirectional solidification without the restriction of traditional rapid solidification preparation conditions [3, 4].

Noticing that strong exothermic reaction due to large negative enthalpy of mixing can occur among major components of the Zr-based bulk metallic glass alloys such as Zr-Al-Ni-Cu (Zr-Ni, Zr-Al, Al-Ni are known alloy systems for high-temperature self-propagating synthesis [5–7]), we developed a new technique to fabricate amorphous-based composite alloys using Laser-induced Self-propagating Reaction Synthesis (LSRS) [8]. Compared with conventional synthesis methods, LSRS uses exothermic reaction to synthesize metastable materials at high heating and cooling rates.

In this paper, microstructure of LSRS products in the $Zr_{55}Al_{10}Ni_5Cu_{30}$ alloy was studied using XRD, SEM and TEM. Hardness and wear resistance of the produced composite alloys are measured and are compared to the single amorphous phase alloy of the same composition.

2. Experimental procedure

Elemental powders of Zr (99.90% purity, −200 mesh), Al (99.90% purity, −200 mesh), Ni (99.90% purity, −200 mesh), and Cu (99.90% purity, −250 mesh) were blended according to the composition of $Zr_{55}Al_{10}Ni_5Cu_{30}$, and then the powder mixture was pressed into a green compact of 8 mm in diameter and 7 mm in height. The ignition was carried out using CO_2laser from above the green compact in an argon atmosphere. The optimized parameters were: laser power 1.2 kW, ignition time 3 s, and beam diameter 8 mm. The typical outlook of a LSRS sample is shown in Fig. 1. The outer surface is smooth and has metallic luster.

The microstructural characterization of the LSRS products was carried out using scanning electron microscopy (SEM) with an energy dispersive X-ray analyzer, transmission electron microscopy (TEM), and X-ray diffraction (XRD). The Vickers hardness in the vertical cross-section of the sample was measured using a load of 0.1 N. The fretting wear test under unlubricated condition was carried out on a SRV testing machine. A bearing steel ball (HRC55) was selected as the wear couple. The experimental parameters were: normal load 20 N, wear time 30 min, slid amplitude 1 mm, and frequency 25 Hz. The widths and morphology of wear scars were examined using SEM, and wear volume V was calculated by the approximate equation [9]:

$$V = \pi d_1^2 d_2^2 / 64R,$$

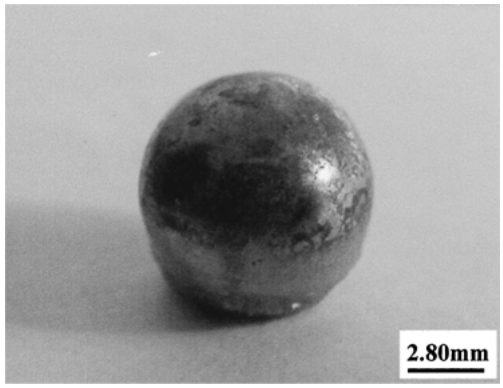

Figure 1 Macro-morphology of the LSRS $Zr_{55}Al_{10}Ni_5Cu_{30}$ alloy.

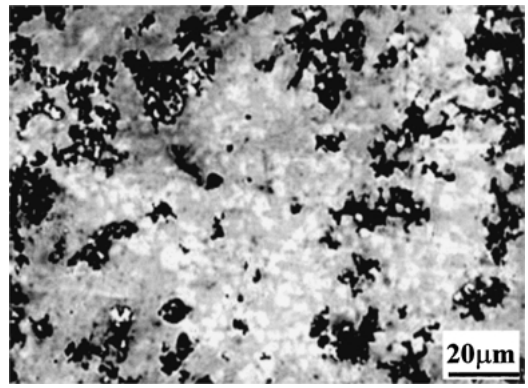

Figure 3 Microstructure of reaction zone of LSRS sample.

where d_1 is the width perpendicular to the fretting direction, d_2 is the width parallel to the fretting direction, and R is the radius of the bearing steel ball.

3. Results and discussions

3.1. Microstructure of the reaction zone

Fig. 2 shows an X-ray diffraction pattern taken from the reaction zone of the sample. It is seen that a broad peak characterizing amorphous phase appears within $2\theta = 35$–45°, on which diffraction peaks corresponding to the Zr_2Cu and Zr_3Al_4 phases superpose. This pattern indicates that the reaction zone mainly consists of amorphous and intermetallics phases.

Fig. 3 shows a typical SEM morphology in the transverse cross-section of the reaction zone, echted with $FeCl_3 + HNO_3$. The microstructure is featured with a fine white block phase, growing in the form of aggregates and inhomogeneously distributing in a gray matrix. The EDX analysis shows that the block phase is the Zr_2Cu intermetallics with chemical composition of $Zr_{65.28}Al_{2.50}Ni_{13.50}Cu_{18.72}$. Furthermore, holes induced by the etching are also found at the brims of the matrix grains, in which enrichment of the Al element is revealed by EDX.

In order to further confirm the formation of the amorphous phase and to identify the types of the crystalline phases, the microstructure of the reaction zone was investigated by TEM. As shown by a bright-field electron micrograph in Fig. 4a, the microstructure is characterized by cellular regions with diameters of 0.8–1.6 μm. Fig. 4b is a magnified photo of Fig. 4a, where the spherical aggregates with an average size of 50 nm inhomogeneously distribute in the matrix with bright contrast. The selected area electron diffraction pattern of this featureless contrast manifests halo rings, typical of an amorphous state (Fig. 4c). The nano-agregates are identified as the C-centered orthorhombic ZrAl compound as indexed in Fig. 4d.

Fig. 5a shows a bright-field electron micrograph from another region. It can be seen that the crystallized regions (assigned as A and B in Fig. 5a) with obvious strain contrast appear besides the cellular regions consisting of the amorphous and nano ZrAl phases (assigned as C in Fig. 5a). Fig. 5b shows a typical selected area electron diffraction pattern of the A region, which is identified as consisting of the body-centered tetragonal Zr_2Cu-type intermetallic, with lattice constants of $a = c = 0.32$ nm, $b = 1.10$ nm. As indexed in Fig. 5c, the selected area electron diffraction pattern of the B region located between two A regions is identified to

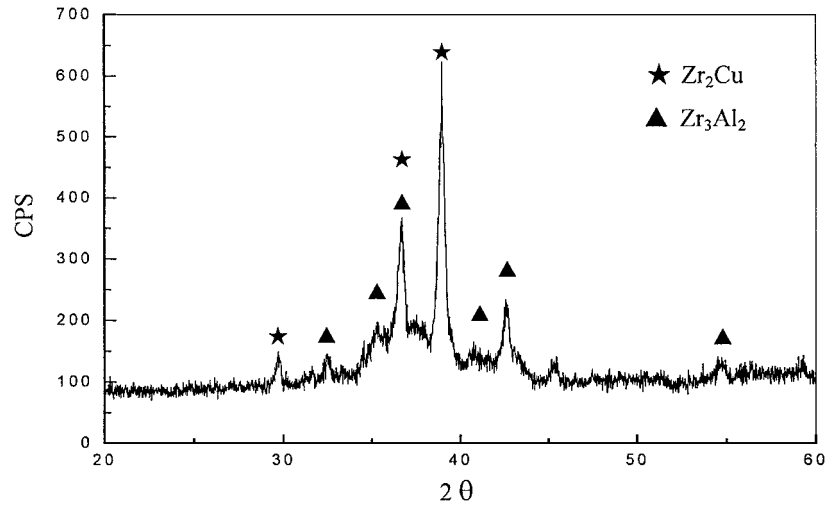

Figure 2 X-ray diffraction spectrum of the Zr-based LSRS sample.

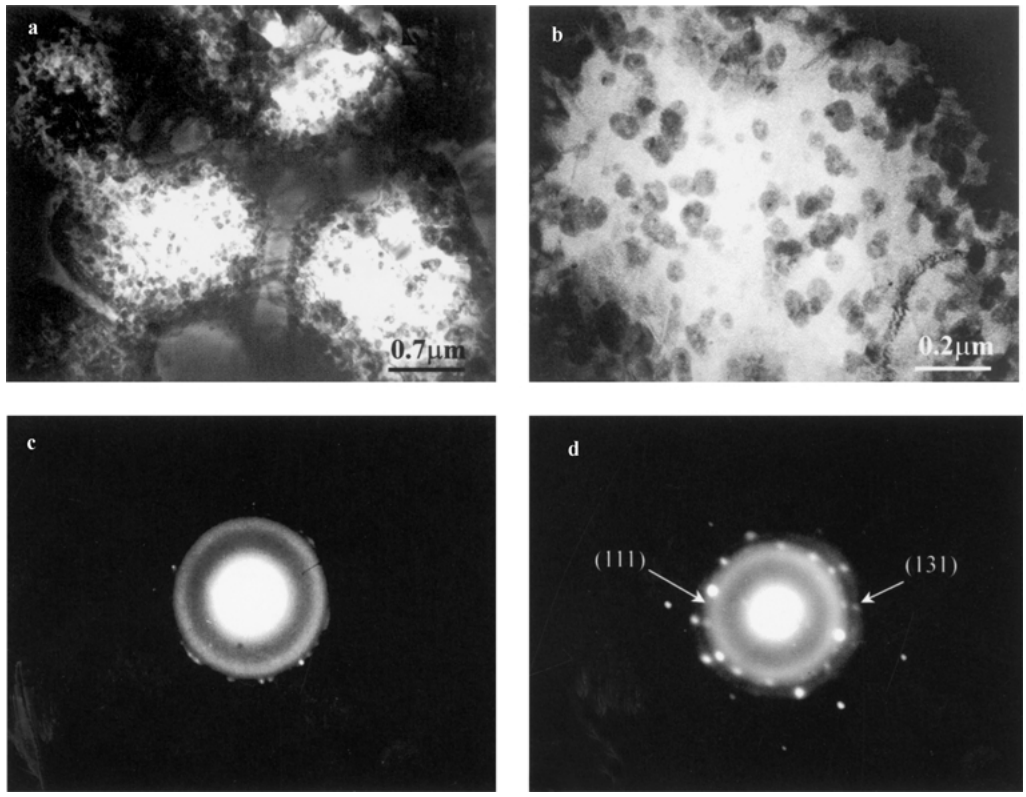

Figure 4 Bright-field image and electron diffraction patterns of the cellular region.

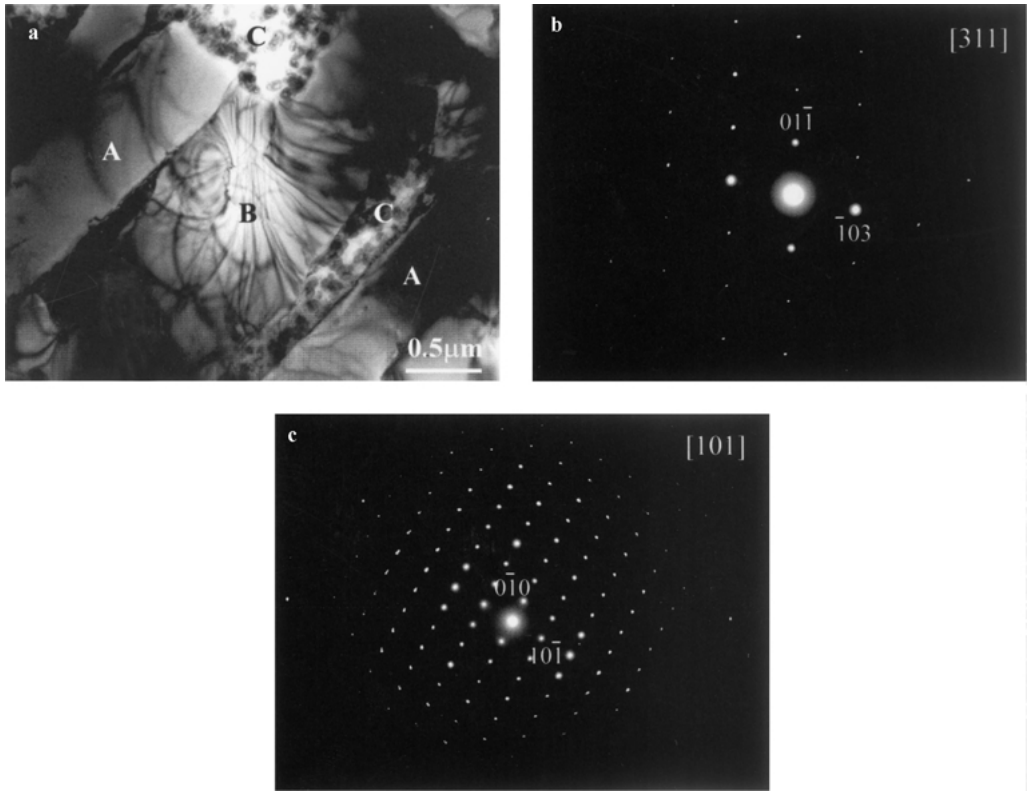

Figure 5 Bright-field image of a region consisting of A: Zr_2Cu (diffraction pattern shown in b), B: Zr_3Al_2 (diffraction pattern shown in c), and C: cellular region.

be the primitive tertragonal. Zr_3Al_2-type intermetallic, with lattice constants of $a = b = 0.76$ nm, $c = 0.69$ nm.

The appearance of multiple phases in the sample is probably due to inhomogeneous raw powder mixtures, to multi-component competing reactions, and to non-equilibrieium thermodynamic processes during the self-propagating reactions.

The exothermal reaction mechanism is still not clear. However, from the fact that a major crystalline phase is the Zr_3Al_2 compound, we can deduct that the reactions

between Zr and Al are the leading exothermal reactions that maintain the self-propagating processes. The Zr_2Cu phase may be formed in secondary reactions because there is no strong exothermal reaction between Zr and Cu. The reactions details are under investigation.

3.2. Microstructure of the laser ignition zone

The X-ray diffraction analysis shows that the laser ignition zone also consists of the amorphous, Zr_2Cu and Zr_3Al_2 phases. However, the reaction process is greatly changed because of the laser's high heat flux density and very rapid heating rate, making the major exothermic reactions more rapid, violent, and complete. The content of the amorphous phase is increased. Fig. 6 shows a bright-field electron micrograph of a cellular region and its corresponding selected area electron diffraction pattern. The amorphous matrix is clean, free of the nano ZrAl aggregates as observed in the reaction zone. Fine twins appear at the brim of the amorphous cell, probably induced by stress.

Another subtle microstructure change is in diversified amorphous morphologies. As shown by the bright-field electron micrograph in Fig. 7a, the amorphous phase has another typical band morphology. Fig. 7b is the corresponding selected area electron diffraction pattern. Furthermore, it is also seen from Fig. 7a that the interface between the amorphous and crystalline phases is not smooth: the crystalline grains grow into the amorphous matrix from the brim.

TABLE I Comparison of the microhardness and wear resistance between the LSRL product and a single amorphous phase alloy of the same composition

	Mcroharsness (kgf/mm^2)	Wear volume (mm^3)
LSRS product	451–487.8	0.171–0.189
Single amorphous phase alloy	342–385	0.270–0.324

3.3. Hardness and wear resistance

Microhardness and wear volume of the LSRL product are given in Table I. For comparison, the data of a single amorphous phase alloy of the same composition obtained by copper mold casting are also shown. It can be seen that the microhardness and the wear resistance of the LSRL product are superior to those of the single amorphous phase alloy due to the presence of the intermetallic phases.

Wear scar morphology of the sample after the fretting experiment for 30 minutes is shown in Fig. 8. Some adhesive substances (assigned as A in Fig. 8a) appear in the central part of a wear scar besides ploughed grooves and detached debris (assigned as B and C in Fig. 8a, respectively). The EDX analysis shows that the adhesive substance is mainly composed of Fe and O, and the chemical composition is $Fe_{28.58}Zr_{12.11}Al_{1.03}Ni_{2.04}Cu_{4.63}O_{51.62}$. This result indicates that material transfer and oxidation occur during the wear process. At the same time, because some of dissociative and hard debris is gradually squeezed out

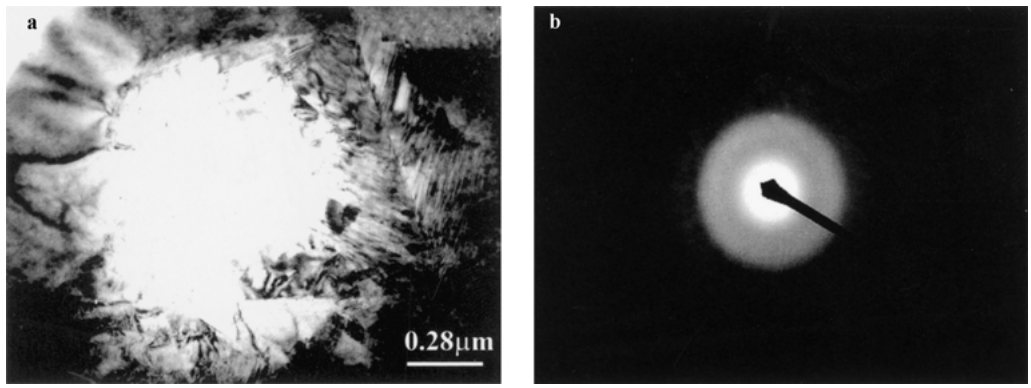

Figure 6 Bright-field image and electron diffraction pattern of a cellular amorphous region from the laser ignition zone.

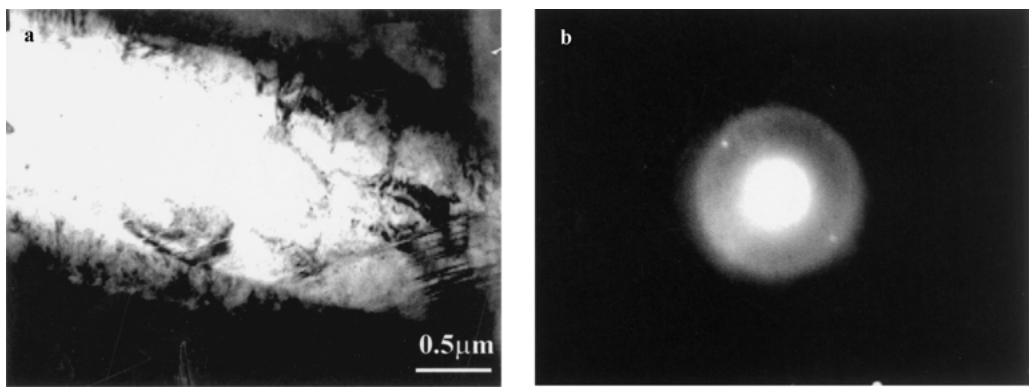

Figure 7 Bright-field image (a) and electron diffraction pattern and (b) of the band-like amorphous.

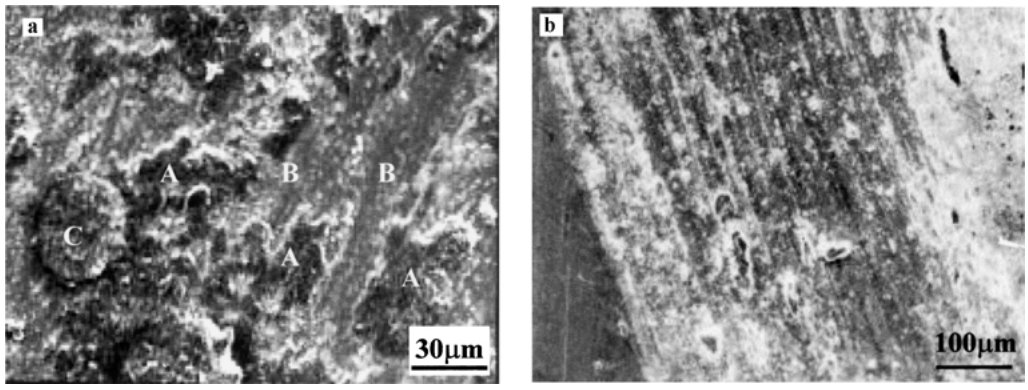

Figure 8 Morphology of worn surface of the LSRS sample. (a) In the central part of the wear scar and (b) in the surrounding area of the wear scar.

from the central part of the wear scar and then joins the wear process as wear particles, abrasive wear with the ploughed groove feature occurs in the surrounding area of the wear scar (as shown in Fig. 8b). It is then inferred that the fretting wear mechanisms are adhesion, oxidation, delamination, and abrasive.

4. Conclusions

A laser-induced self-propagating reaction synthesis method has been successfully applied in the fabrication of an amorphous-based composite $Zr_{55}Al_{10}Ni_5Cu_{30}$ alloy. The product mainly consists of the amorphous, Zr_3Al_2 and Zr_2Cu phases. In the reaction zone, the amorphous phase has a typical cellular morphology, imbedded with nano ZrAl aggregates with an average particle size of 50 nm. More amorphous content is found in the laser ignition zone because of the laser's high heat flux density and very rapid heating rate. Microhardness and wear resistance of the product are superior to those of a single amorphous phase sample obtained by copper mold casting due to the presence of the intermetallic phases.

Acknowledgment

The present work is supported by National Science Foundation of China under grant no. 50271012.

References

1. A. INOUE, *Acta Materialia* **48** (2000) 279.
2. A. INOUE, T. ZHANG and T. MASUMOTO, *J. Non-Crys. Solid* **156–158** (1993) 473.
3. *Idem.*, *Material Transactions* **36** (1995) 391.
4. A. INOUE, Y. SHINOHARA, Y. YOKOYAMA and T. MASUMOTO, *ibid.* **36** (1995) 1276.
5. N. CHIKASHI, A. MUNEGYUKI and K. YOSHINARI, *ibid.* **31** (1990) 471.
6. G. SIPNOLO, G. FLOR and Z. A. MUNIR, *Journal of Alloys and Compounds* **247** (1997) 190.
7. Y. LU and M. HIROHASHI, *J. Mater. Sci. Lett.* **18** (1999) 395.
8. C. S. WANG, G. LI, Y. L. XIA and C. DONG, Chinese Patent no. 01106093. X (2001).
9. G. Z. XU, Z. R. ZHOU and J. J. LIU, *Wear* **224** (1999) 211.

Received 4 October
and accepted 24 December 2002